ELSEVIER

Polymer 42 (2001) 563–575

polymer

www.elsevier.nl/locate/polymer

Molecular relaxation study of polystyrene: influence of temperature, draw rate and molecular weight

L. Messé, M. Pézolet, R.E. Prud'homme*

Département de chimie, Centre de recherche en sciences et ingénierie des macromolécules, Université Laval, Québec, Canada G1K 7P4

Received 17 February 2000; received in revised form 18 May 2000; accepted 19 May 2000

Abstract

Molecular relaxation curves of five different polystyrene samples, four monodisperse of weight-average molecular weight ranging from 210 000 to 2 340 000, and one polydisperse, have been studied using birefringence and polarization modulation infrared linear dichroism, during and after a step-strain uniaxial deformation at temperatures between T_g and $T_g + 60$°C. Relaxation measurements can be fitted with a set of exponential decay functions, thus defining three different relaxation times. The relaxation times thus obtained with birefringence and polarization modulation experiments are similar, and decrease with an increase in temperature. The first relaxation time (τ_1), which is of the order of seconds, is independent of average molecular weight (M_w), while the second (τ_2) and third (τ_3) relaxation times increase with molecular weight. For example, at $T_g + 20$°C, and for a PS molecular weight of 2 340 000, values of 0.7, 39 and 16 500 s were determined for τ_1,τ_2 and τ_3, respectively. The power law dependence found for the third relaxation time scales as $M_w^{1.6}$ at each temperature. This behavior is consistent with the prediction of the theoretical model of Doi–Edwards and allows the assignment of τ_1 to the first, and τ_3 to the second relaxation time of Doi–Edwards (τ_2 is intermediate between those two). The decrease of the relaxation time ratio (τ_3/τ_1) with temperature, noted for all the PS molecular weights investigated, suggests a decrease in the number of entanglement points with an increase in temperature above $T_g + 20$°C. Finally, for a given temperature, a linear dependence is observed between τ_3 and τ_1 in agreement with the $\tau_3 = 2\tau_1 N^{1.6}$ Doi–Edwards prediction, where N is the number of entanglements. © 2000 Elsevier Science Ltd. All rights reserved.

Keywords: FTIR spectroscopy; Polarization modulation; Birefringence

1. Introduction

The determination of relaxation times after a large deformation, and their temperature and molecular weight dependencies, is an essential step in understanding the relaxation mechanisms governing chain dynamics. Experimentally, numerous attempts have been made to determine the segmental motions in linear amorphous homopolymers and binary blends from rheological [1,2] and chain diffusion studies [3–6], but with limited success. Actually, several experimental techniques have allowed observing and quantifying to a certain extent the molecular relaxation of polymer chains at long times [6–14], but short relaxation times could be obtained from indirect determinations only, deduced from either orientation measurements or long relaxation times, assuming the validity of the Doi–Edwards model [6–8,15–19]. Theoretically, the chain diffusion [20–23] is described by a reptation process [24] inside a tube-like environment defined by the surrounding topological constraints and imposed by the neighboring chains.

According to the Doi–Edwards theory [25–28], the successive relaxation processes of an amorphous polymeric material in an entangled environment can be divided into three well-separated relaxation steps: first, a fast relaxation in which the equilibrium between two successive entanglement points, within the deformed tube, is reached through local rearrangements by 'Rouse-like' motions. The corresponding relaxation time τ_a is assumed to be molecular weight (M) independent; second, there is a recoil of the chain ends inside the deformed tube in order to reduce the total contour length of the primitive chain down to its original value prior to deformation. This phenomenon is assumed to occur in a time, τ_b, which scales with M^2; and third, the chain disengages from its initial tube via a reptation process in order to restore an isotropic configuration in the medium. This terminal relaxation time, τ_c, scales with M^3.

One important experimental limitation in the determination of relaxation times is that the initial relaxation processes, at times smaller than 100 s, are difficult to

* Corresponding author.
E-mail address: prudhomme@chm.ulaval.ca (R.E. Prud'homme).

0032-3861/01/$ - see front matter © 2000 Elsevier Science Ltd. All rights reserved.
PII: S0032-3861(00)00394-3

Table 1
Characteristics of the polystyrene samples used

	M_w	M_w/M_n	T_g (°C)	Sources
PS2M	2 340 000	<1.3	107	Pressure chemicals
PS900	942 000	<1.1	105	Pressure chemicals
PS650	670 000	<1.1	105	Pressure chemicals
PS400	400 000	<1.06	104	Pressure chemicals
PS210	210 000	2.1	96	Dow chemicals

measure accurately with the conventional techniques. For example, with infrared spectroscopy, the relaxation curves measured are either generated from different samples, after the necessary heating and quenching steps, or recorded during the relaxation using the conventional linear dichroism technique that requires the acquisition of two successive spectra with different polarization states of the infrared radiation. In every case, during the cooling stage or the polarizer rotation, significant relaxation of the sample occurs, which alters the short relaxation time measurement.

This problem can be circumvented with the polarization modulation infrared linear dichroism (PM-IRLD) technique [29,30] for which a fast change of the state of polarization of the incident infrared light beam is produced by a photoelastic modulator [31–33]. As compared to the classical infrared linear dichroism method where a maximum accuracy of the order of 0.01 units [6,10–12] is obtained for the orientation function, $\langle P_2(\cos\theta)\rangle$, the PM-IRLD technique is able to follow accurately rapid changes of the segmental anisotropy [34,35]. Dichroic differences as low as 2×10^{-4} were detected for poly(dimethyl siloxane) using this technique [36]. Measurements at short times then become available to develop and verify models in order to improve our understanding of the relaxation phenomena of amorphous entangled polymers.

In this article, relaxation measurements of four monodisperse and one polydisperse polystyrenes (PS) of different molecular weights, deformed between $T_g + 4$ and $T_g + 60$°C, have been made using two different experimental techniques following a rapid deformation, up to a draw ratio of 2. First, infrared measurements were made with the PM-IRLD technique, giving data points of high accuracy, at a rate more than 10 times faster than the linear dichroism method; second, birefringence measurements were carried out at a rate of 500 data points per second. These two intrinsically different and independent methods could then be validated one against the other. In studies on polymer blends (involving PS as one of its components [37]), the PM-IRLD technique should, however, be preferred because birefringence cannot provide independently the relaxation curves of the two components involved. Here, the relaxation curves obtained with these two methods, which are in excellent agreement, led to the determination of three temperature-dependent relaxation times, which have been compared and discussed with values expected from the Doi–Edwards model and reported in the literature.

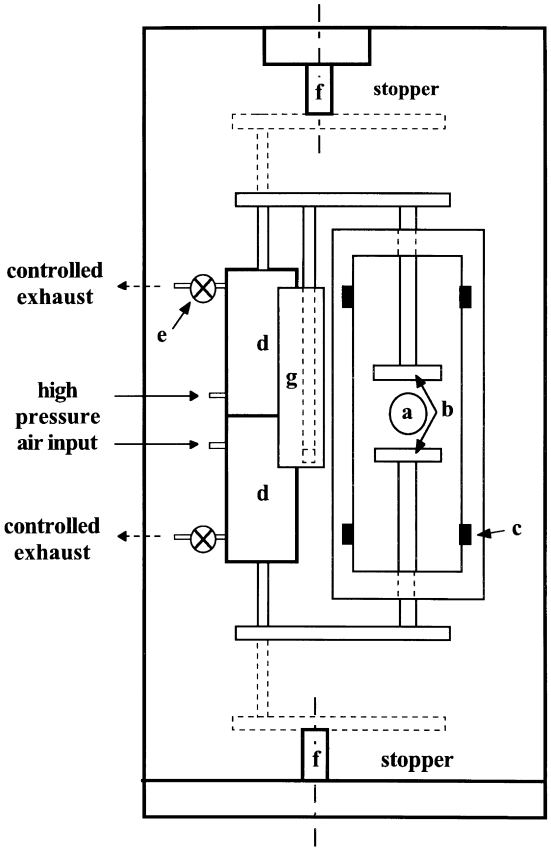

Fig. 1. High speed pneumatic stretching device: (a) ZnSe window; (b) jaws; (c) cartridge heaters; (d) double-acting cylinders; (e) fine metering valves; (f) stoppers; (g) slotted optical switches.

2. Materials and methods

2.1. Sample preparation

Five atactic polystyrene (PS) samples were used, four were monodisperse and the other polydisperse. Their characteristics, in terms of weight-average molecular weight (M_w), polydispersity index (M_w/M_n) and glass transition temperature (T_g), are summarized in Table 1. T_g was determined by differential scanning calorimetry from the midpoint of the heat capacity jump at a heating rate of 20°C/min. PS films, suitable for both the infrared and birefringence studies, were prepared by solution casting of a 6% chloroform solution onto a glass plate. After two days of air-drying, thin films of 50–100 μm in thickness were slowly heated above T_g under vacuum for two more days, to remove any trace of solvent and internal stresses. The resulting samples were cut into strips of about 20 mm in length and 6 mm in width. Prior to stretching, the residual birefringence was verified with a Babinet compensator method and the infrared dichroic ratio technique: in every case, no initial orientation could be detected. After stretching, the final draw ratio was verified from ink marks previously made on the strip. Infrared measurements on stretched PS

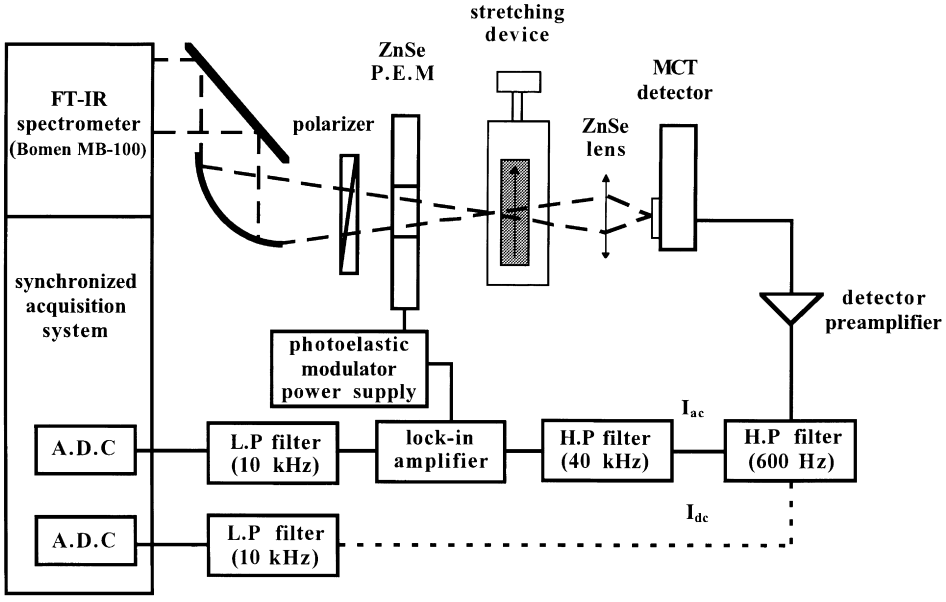

Fig. 2. Schematic diagram of the polarization modulation IRLD set-up.

samples were made using the 906 cm^{-1} infrared band. This band, assigned to the out-of-plane υ_{17b} mode of the phenyl ring, is considered to be conformationally insensitive [38] and has been largely used in the past to study PS orientation in both homopolymers [39,40] and PS-based blends [41,42].

2.2. Stretching devices

Two stretching devices were used to deform the PS samples, at constant draw rate, over a temperature range between $T_g + 4$ and $T_g + 60$°C. A mechanical stretcher was used in the lower range of temperature at and below $T_g + 20$°C, whereas a fast pneumatic stretching device (Fig. 1) was employed for relaxation studies above $T_g + 20$°C, with a few representative temperatures done with both devices. The pneumatic stretching machine, which allows a sample deformation in less than 10 ms, was designed and built in our laboratory. It uses pressurized air ($P = 6$ bar) to push two double acting compact cylinders, d (Festo, ADVUL,39-50-PA), simultaneously, over a distance determined by the two stoppers, f. The maximum force delivered by these two cylinders is 483 N at 6 bar. The draw ratio can be varied from 1.5 to 3 by 0.5 steps by changing the stoppers. Four cartridge heaters, c (Omega, CIR), maintain the temperature inside the chamber between 40 and 200°C (±0.5°C), as monitored by a temperature controller (Omega, CN 76000). The draw rate, which is linear, is monitored by the control of air speed exhausts through two fine metering valves, e (Nupro, M), and measured with a row of 12 slotted optical switches, g (TRW elec., OPB804). The lowest stretching speed obtained with the pneumatic system is 50 m/min while, with the mechanical device, the maximum speed available is of 10 cm/min. In all relaxation experiments, the draw ratio was fixed at 2.

2.3. Birefringence measurements

The deformation of an amorphous polymeric sample gives rise to two well-known correlated optical material properties: birefringence and dichroism. Birefringence is defined as the anisotropy in retardation between the two light components passing through the stretched sample, whereas dichroism is related to the anisotropy of attenuation of the polarized infrared radiation within the material. In the case of an amorphous homopolymer, the birefringence, Δn, and the average of the second Legendre polynomial, $\langle P_2(\cos\theta)\rangle$, characteristic of the segmental orientation obtained by infrared linear dichroism, are directly proportional [43,44]:

$$\Delta n = \langle P_2(\cos\theta)\rangle \Delta n^{\circ} \quad (1)$$

where Δn° is the intrinsic birefringence of the material.

In this work, a birefringence apparatus similar to that developed by Kumar and Stein [45] was built to follow the material birefringence during the orientation and relaxation periods as a function of time t. The signal I varies sinusoidally with the sample deformation and is related to the birefringence Δn through:

$$I = I_0 \sin^2((\pi d \Delta n)/\lambda_0) \quad (2)$$

where d is the thickness of the sample (corrected with elongation, assuming an affine deformation) and λ_0, the wavelength of the incident light of intensity I_0. In this birefringence set-up, a helium–neon laser source ($\lambda_0 = 632.8$ nm), two silicon photodiodes (Melles Griot), the Labview® software and a Pentium PC were used for fast data acquisition. The maximum scanning rate available with the conversion card selected was 50,000 points/s. Typically, at the beginning of the experiment, one data point was

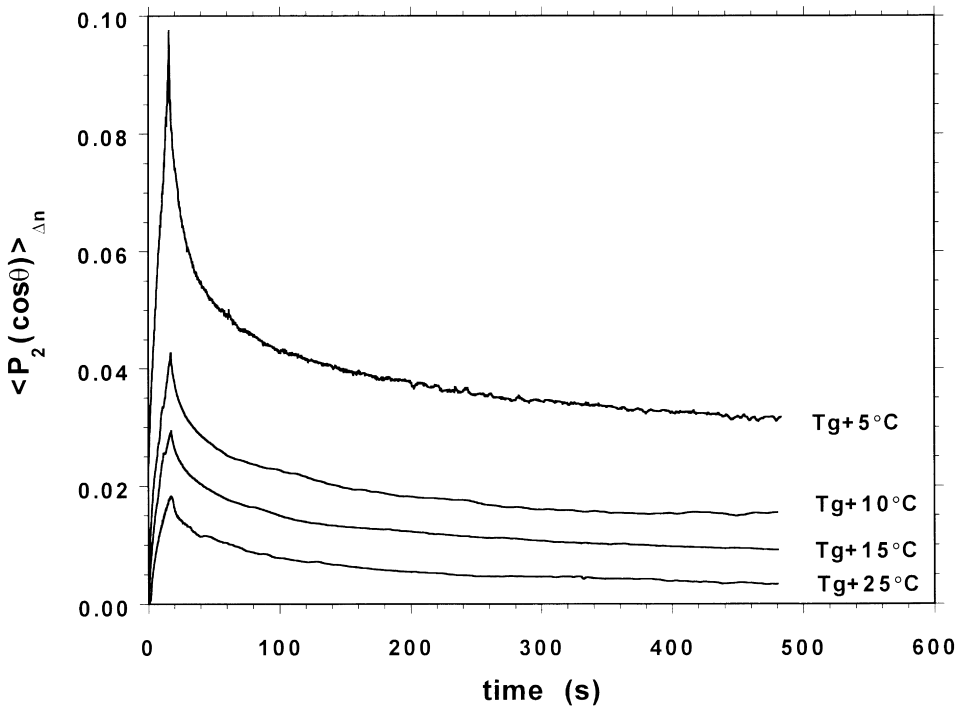

Fig. 3. Orientation and relaxation birefringence curves of polydisperse PS, at different temperatures, after linear deformation at a constant draw rate of 10 cm/min.

recorded every 2 ms while, at longer times, the number of data points was reduced to one point every second. The analysis, converting $I(t)$ into $\Delta n(t)$, was carried out with Microsoft Excel®. The mechanical stretcher, also used in the PM-IRLD experiments, allows a constant temperature to be maintained above the PS T_g and gives constant draw rates up 10 cm/min.

2.4. Polarization modulation IR measurements

For the PM-IRLD method, a Bomen Michelson MB-100 spectrometer was used with the optical set-up shown in Fig. 2 and the two-channel electronic processor described previously [34]. Briefly, the infrared beam at the output of the interferometer, already modulated at low frequency by the interferometer moving mirror, is first polarized along the stretching direction with a wire-grid polarizer and, then, by the photoelastic modulator at a frequency of 74 kHz, before hitting the sample and being focused and collected onto the mercury–cadmium–telluride detector. The signal at the output of the detector, containing the information about the intensity and polarization modulation, is pre-amplified and then divided into two signals, I_{ac} and I_{dc}, using proper electronic filtering. The high-frequency polarization modulation signal is demodulated with a lock-in amplifier (EG&G instruments, 7260 DSP) synchronized with the photoelastic modulator. Finally, the two signals are sent to two ADCs that are simultaneously sampled by a digital signal processor interface and FFT board to give I_{ac}/I_{dc}. By using a proper calibration procedure, this ratio allows the quantitative determination of the dichroic difference spectrum of the oriented sample ($\Delta A = A_{\parallel} - A_{\perp}$), from which the sample orientation is calculated [36,46,47]:

$$\langle P_2(\cos\theta)\rangle = \frac{3\langle\cos^2\theta\rangle - 1}{2} = \left(\frac{R_0 + 2}{R_0 - 1}\right)\left(\frac{\Delta A(\lambda)}{3A_0}\right)\sqrt{\lambda} \quad (3)$$

with $R_0 = 2\cot^2\alpha$, and where α is the angle between the transition moment of the vibrational mode considered with respect to the chain axis ($\alpha = 35°$ for the 906 cm^{-1} band [38]), A_0 is the absorbance of the isotropic sample and λ the draw ratio. The modulation conditions and apparatus were the same as those reported in Refs. [25–28]; the only parameters changed were the moving mirror speed ($v =$ 1.012 cm/s), the resolution (8 cm^{-1}), the filter limits (displayed in Fig. 2), the time constant ($\tau = 20\ \mu s$) and the number of scans per spectrum. This last parameter varied from 10 scans/spectrum in relaxation up to 15 scans/spectrum in orientation, which corresponds to one point every 4 and 6 s, respectively. The wavenumber selected on the modulation controller was adjusted at 1100 cm^{-1} to give a maximum efficiency of the modulator in the frequency range of interest.

From birefringence and PM-IRLD experiments, pre-exponential parameters and relaxation times were determined with Microsoft Excel®, which uses an advanced Newtonian method to optimize the least-squares difference between the experimental and calculated curves.

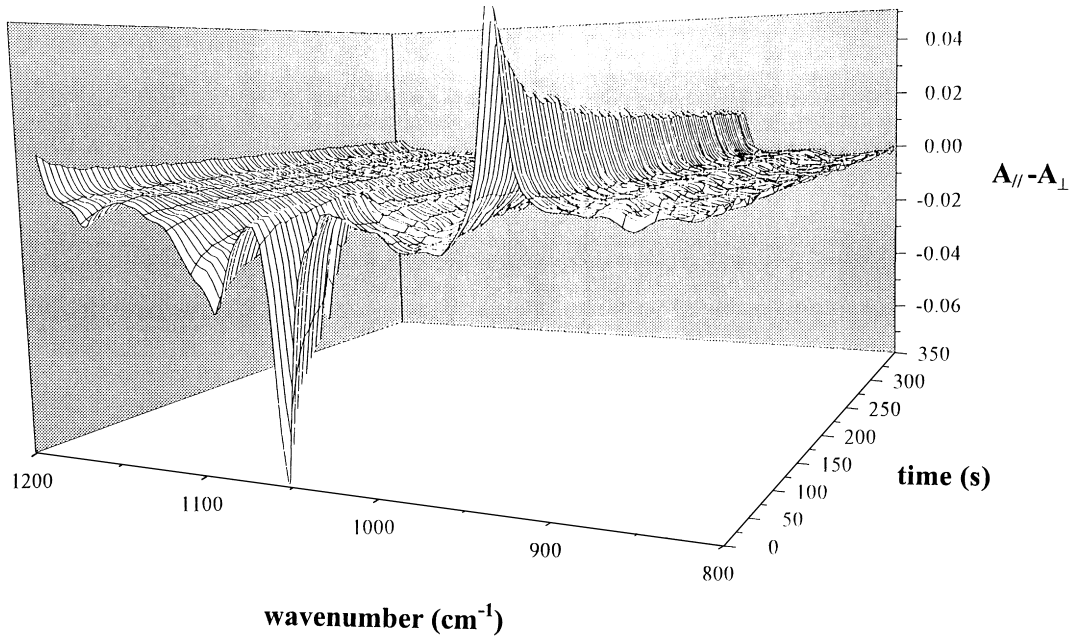

Fig. 4. Evolution of the difference dichroic infrared spectrum of polydisperse PS as a function of time, after a deformation at a constant draw rate of 10 cm/min ($\lambda = 2$; the photoelastic modulator was set at 1100 cm^{-1}).

3. Results

The orientation behavior of PS was first investigated as a function of draw rate and temperature, above T_g, by the birefringence and PM-IRLD techniques [37], but these results will not be shown here because similar results can already be found in the literature [15–18,38–42]. However, a direct comparison between the birefringence and PM-IRLD data indicated that the PS intrinsic birefringence remains constant in the temperature and draw rate intervals covered [37]. Then, using Eq. (1), the $\langle P_2(\cos\theta)\rangle$ values determined by PM-IRLD and the Δn values measured by birefringence, an average intrinsic birefringence value of -0.095 ± 0.005 was obtained, in agreement with the calculated average value of -0.10 previously reported [48] (with an excessively large uncertainty of ± 0.05), and also with the experimental value of -0.12 reported by Jasse and Koenig [38], and with the -0.08 value of Abtal [49].

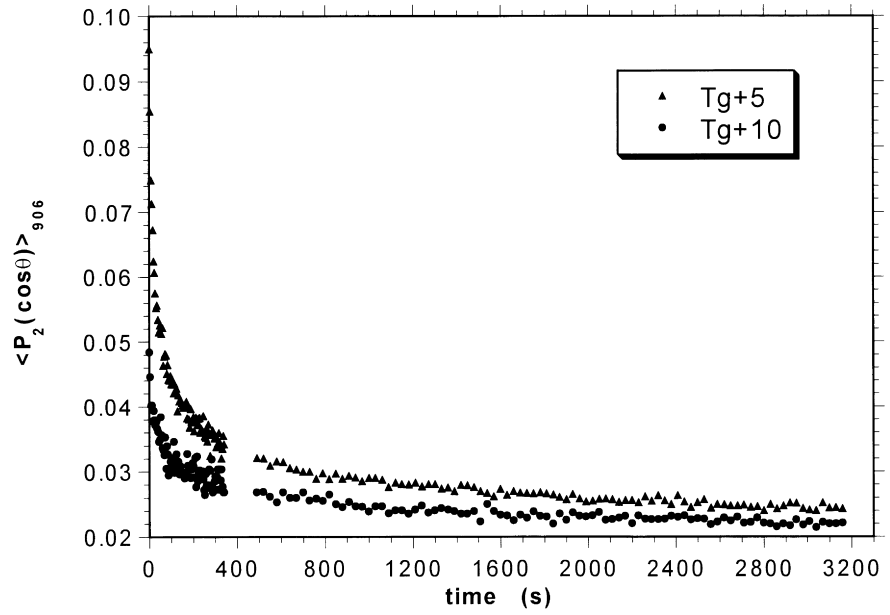

Fig. 5. PM-IRLD relaxation curves of polydisperse PS obtained using the 906 cm^{-1} band, at a constant draw rate of 10 cm/min and at $\lambda = 2$. Note that, in each curve, a gap occurs between 360 and 460 s due to computer memory limits, obliging us to make a second acquisition run as soon as the first one stopped.

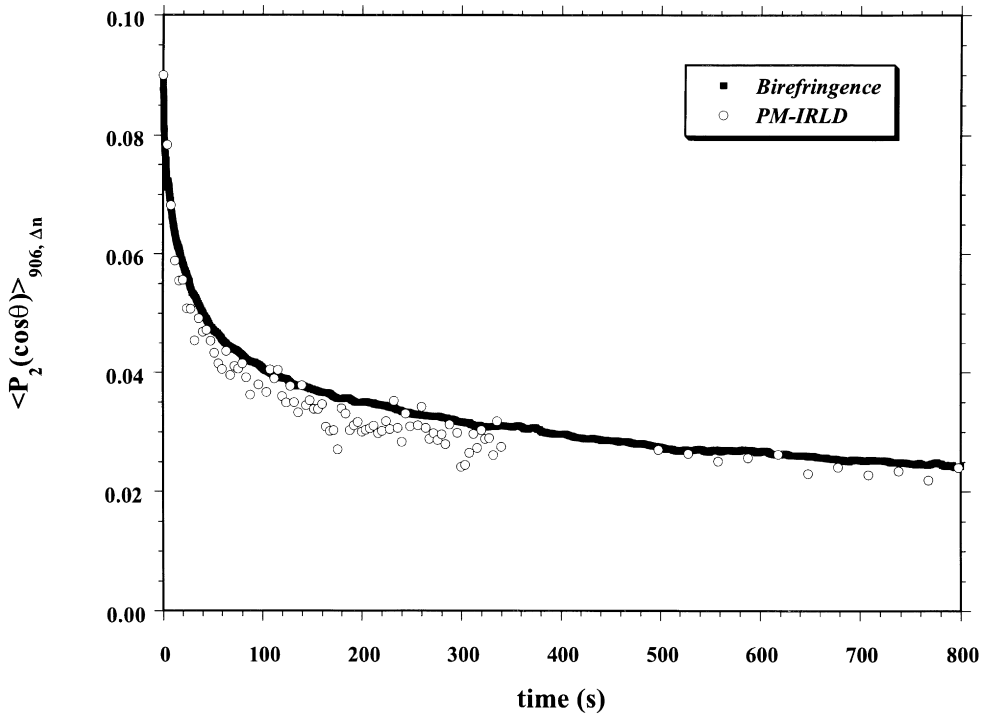

Fig. 6. Comparison of birefringence and PM-IRLD relaxation curves as a function of time, at T_g + 5°C, for polydisperse PS.

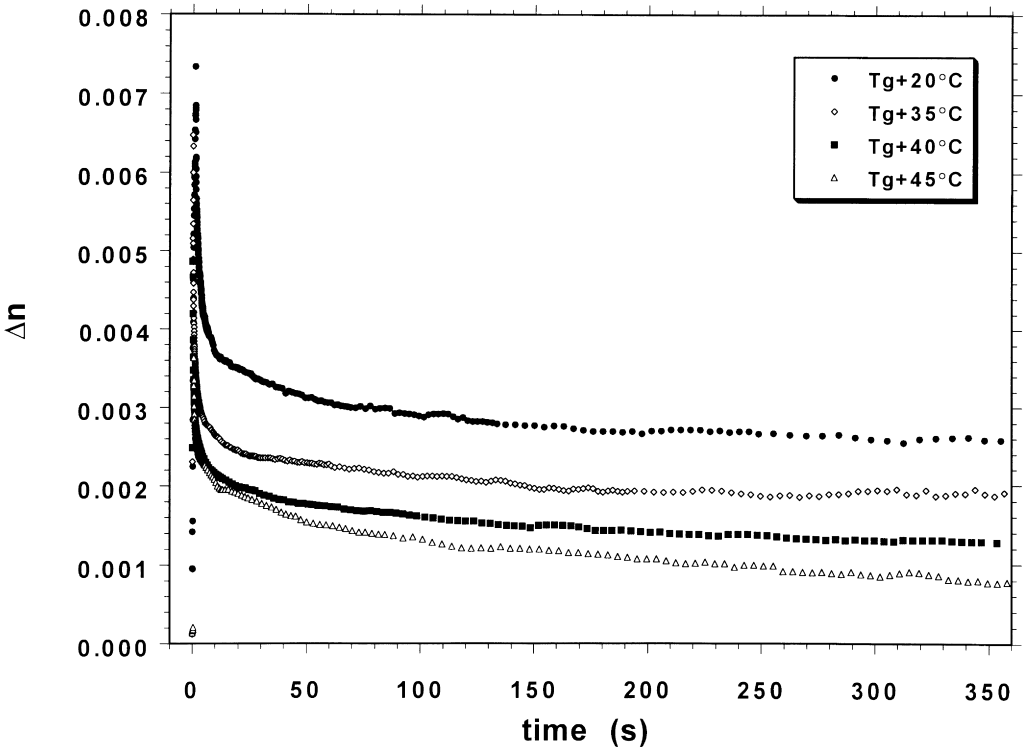

Fig. 7. Birefringence curves during the orientation and relaxation of monodisperse PS as a function of time, at two different temperatures (draw rate = 50 m/min, $\lambda = 2$, $M_w = 2\,340\,000$) run with the pneumatic stretcher.

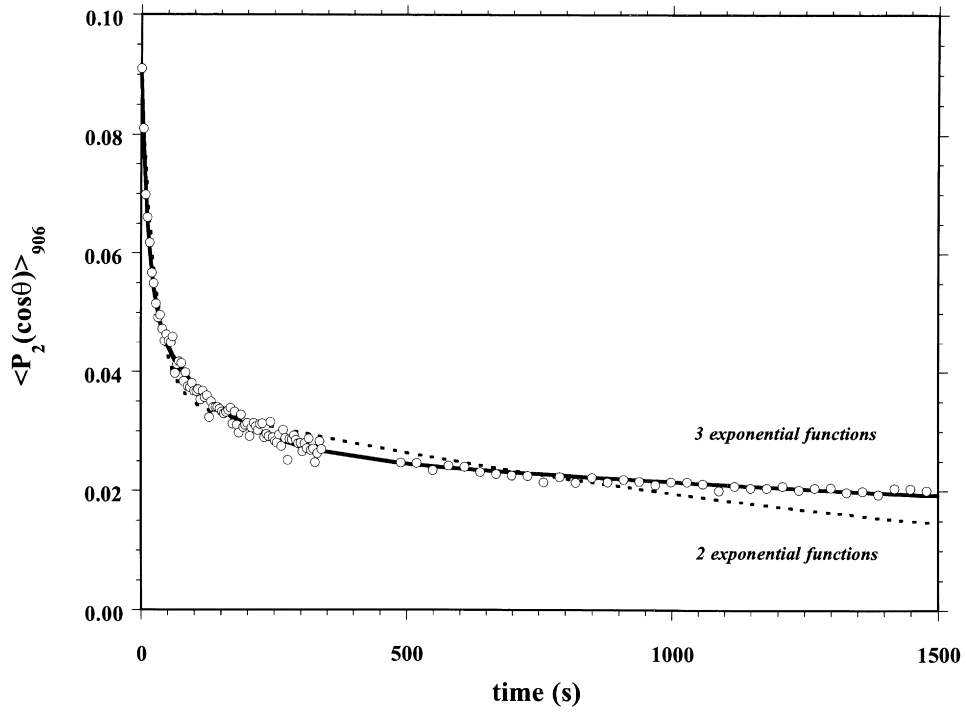

Fig. 8. Exponential decay functions containing two and three terms (birefringence relaxation curve recorded at T_g + 5°C).

From our experimental value and using Stein's equation [50], a constant angle of 41 ± 1° was calculated between the perpendicular of the plane of the phenyl ring and the chain axis, for the range of temperatures and draw rates investigated.

Relaxation curves, determined from birefringence after an elongation up to $\lambda = 2$ at a draw rate of 10 cm/min, are reported in Fig. 3 for the polydisperse PS as a function of time, at four different temperatures (the measured birefringence values were converted to orientation functions using Eq. (1) and the intrinsic birefringence value of −0.095 determined above). Each of the curves exhibits an exponential decay with respect to time (after the deformation, which gives the initial increase) and can be decomposed into two parts: a fast exponential decrease at short times and a slow decrease at long times. With an increase in temperature, the relaxation process becomes faster and, at long times, the $\langle P_2(\cos\theta)\rangle$ values get closer to zero.

In order to confirm this behavior, the PM-IRLD spectra of the polydisperse PS, recorded between 800 and 1200 cm^{-1}, were also made at different temperatures. Dichroic difference spectra, determined at T_g + 10°C, as a function of time and wavenumber, are shown in Fig. 4. With time, it is seen that the dichroic difference, which can be either positive or negative depending upon the orientation of the transition moment with respect to the chain axis, decreases for all the infrared bands recorded. The orientation relaxation curves obtained from such spectra, using the 906 cm^{-1} band, are reported in Fig. 5, at two temperatures. When the temperature increases, at short times, the $\langle P_2(\cos\theta)\rangle$ values decrease more rapidly with time due to an increase in chain mobility and, as for birefringence, they get closer to zero.

A comparison of the relaxation curves, recorded from the birefringence and the PM-IRLD techniques, at T_g + 5°C, is shown in Fig. 6. Within the experimental error, the two curves exhibit similar behavior and, therefore, give access to similar information about the PS relaxation processes. At each temperature, agreement is found between birefringence and PM-IRLD relaxation curves, including the same plateau at long times (if the non-translated curves are considered). However, with the experimental conditions selected for the PM-IRLD experiments, the temperature range was limited to T_g + 10°C since, above this temperature, the relaxation process was too fast to provide reliable determination of the relaxation time. Since the birefringence technique allows a rapid data acquisition, relaxation curves up to T_g + 20°C (not shown in the figure) were recorded from which reliable relaxation times could be easily calculated.

By using the pneumatic stretcher which allows stretching of polymer films at a draw rate of 50 m/min, birefringence relaxation curves of PS were recorded up to T_g + 60°C. As an example, the birefringence relaxation curves of a 2 340 000 monodisperse PS are shown in Fig. 7, at four different temperatures. As the temperature increases, the maximum birefringence, resulting from the chain orientation (at time 'quasi-zero'), decreases due to the higher level of relaxation during stretching. All relaxation curves decrease steeply in the first 10 s and, then, more slowly

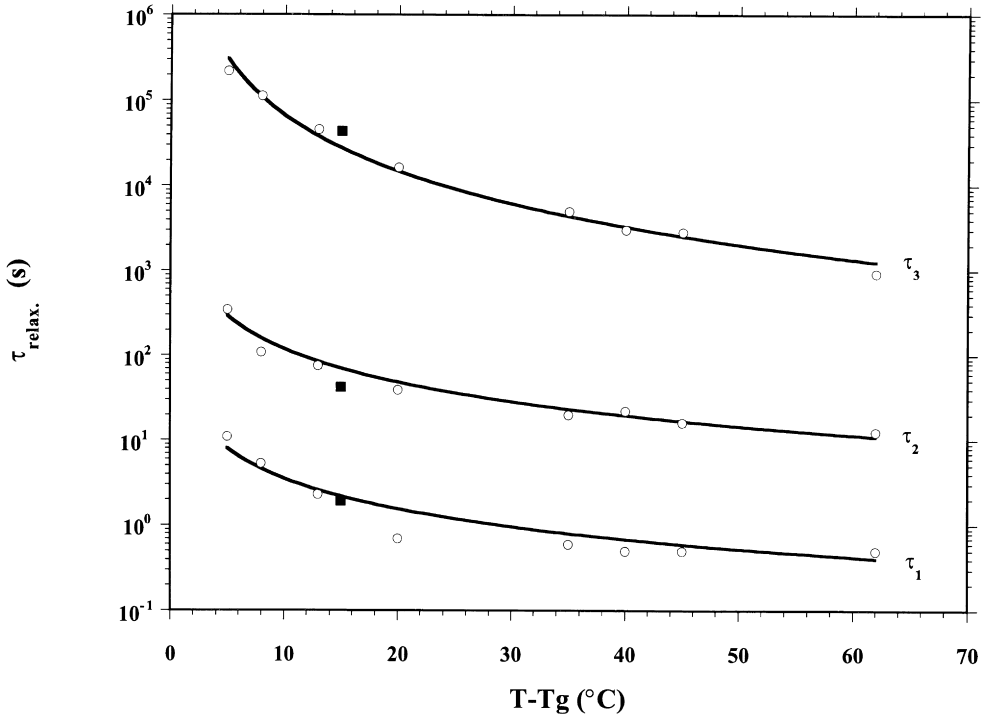

Fig. 9. Variation of the PS relaxation times (τ_1, τ_2, τ_3) as a function of relative temperature above T_g ($M_w = 2\ 340\ 000$, $\lambda = 2$) (Data represented by full square symbols were obtained with the pneumatic device in a temperature zone where the mechanical stretcher was otherwise used, see text).

between 10 and 60 s, followed by an additional very slow relaxation process at longer times. It should be mentioned that, below $T_g + 20$°C, the behavior of the relaxation curves measured following deformation at draw rates of 10 and 50 m/min, with the (slow) mechanical and (fast) pneumatic stretchers, respectively, are the same. However, at and above $T_g + 20$°C, they are different most likely because there is more relaxation during the deformation and, therefore, the use of the pneumatic stretching device is required. Above $T_g + 60$°C, no relaxation curves could be recorded due to the sample breakage after a few minutes during the relaxation period.

The relaxation curves shown in Fig. 7 cannot be superposed, as is usually done with mechanical relaxation data, by shifting the curves along the log(time) axis. When this is attempted, the rapid decrease of birefringence at short times always deviates from the master curve and it is impossible to obtain a satisfactory superposition at short and long times, simultaneously. In other words, time–temperature superposition can only be obtained with the data obtained at long times, i.e. above 10–20 s, but not below it.

4. Discussion

From the relaxation curves shown in the previous section, relaxation times can be determined directly if an appropriate function is used. In this work, we have selected exponential functions, as suggested by the Doi–Edwards theory [25–28]:

$$P_2(t) = \sum_{i=1}^{n} A_i \exp(-t/\tau_i) \tag{4}$$

where $P_2(t)$ is the orientation function at time t, A_i the pre-exponential factor and τ_i the relaxation time. A representative example, using a PM-IRLD relaxation curve, is shown in Fig. 8. It is clear that the use of three exponential terms leads to a satisfactory agreement with the experimental data while, on the contrary, poor agreement is reached with only two exponential terms whereas the choice of four exponential terms leads to no significant improvement. An extended exponential [36] was also considered to fit the relaxation curves but rejected since no linear dependence is observed when $\ln(-\ln(P_2(t)/P_2(0)))$ versus $\ln(t)$ is plotted for both the birefringence and PM-IRLD data. The addition of a simple exponential term to the extended exponential leads to a constant value of the first relaxation time with an increase in temperature, which is unreasonable. Finally, a hyperbolic function was also rejected since it gives poor agreement between the experimental and the calculated curves. A sum of three exponential terms, as expressed in Eq. (4), was then used for all samples. On the other hand, all attempts to use deconvolution methods, as done in viscoelastic experiments such as mechanical stress relaxation functions, failed.

The three relaxation times determined from birefringence

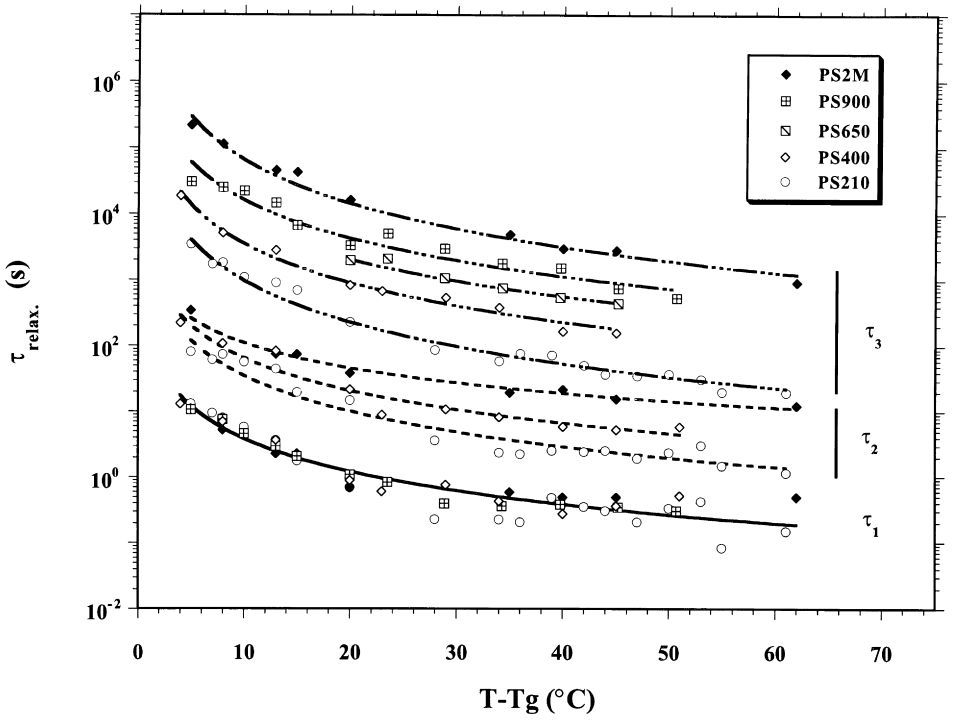

Fig. 10. Variation of relaxation times as a function of temperature, for the PS samples with different molecular weights (the τ_2 data for molecular weight of 900 000 and 650 000 are not shown for clarity).

curves for the monodisperse PS of weight-average molecular weight of 2 340 000 are shown in Fig. 9 as a function of temperature on a semi-logarithmic scale. They decrease with the increase in temperature but more rapidly between T_g and $T_g + 20$°C than above $T_g + 20$°C. The first (τ_1) and second (τ_2) relaxation times vary similarly, while the third (τ_3) relaxation time exhibits a more pronounced decay. It is recalled that the data points shown at $T_g + 20$°C or below were obtained using the (slow) mechanical stretching machine whereas those above $T_g + 20$°C were generated with the (fast) pneumatic stretcher. However, the relaxation times represented by dark square symbols in Fig. 9, at $T_g + 15$°C, obtained using the pneumatic stretcher, clearly demonstrates that the values obtained are independent of the stretching device used.

Fig. 10 shows the variation of the three relaxation times, τ_1, τ_2, τ_3, of the five PS investigated, as a function of temperature, on a semi-logarithmic scale. All relaxation times decrease with the increase of temperature and with the decrease in molecular weight, except for the first relaxation time, which is independent of the molecular weight and polydispersity. The relaxation time–temperature dependence was fitted with a Vogel–Fulcher–Tammann (VFT) equation [51,52]:

$$\ln \tau_i = A + \frac{B}{(T - T_g) + (T_g - T_\infty)} \quad (5)$$

Table 2
Relaxation times (τ_1, τ_2, τ_3) and pre-exponential parameters (A_1, A_2, A_3) determined from birefringence and PM-IRLD relaxation curves, at different temperatures above T_g

Methods	$T - T_g$ (°C) (±0.5)	τ_1 (s) (±1)	τ_2 (s) (±15)	τ_3 (s) (±200)	A_1 (±0.005)	A_2 (±0.005)	A_3 (±0.005)
IR.	4	16	95	4230	0.050	0.030	0.035
Bir.	5	13	80	3540	0.034	0.021	0.032
IR.	5	14	105	3770	0.038	0.025	0.025
Bir.	7	10	65	1750	0.026	0.021	0.032
Bir.	8	8	75	1845	0.019	0.021	0.026
IR.	8	9	85	2530	0.016	0.020	0.020
Bir.	10	6	55	1300	0.011	0.016	0.021
IR.	10	6	65	1390	0.008	0.015	0.015
Bir.	13	4	45	1010	0.006	0.012	0.021
Bir.	15	2	20	700	0.006	0.011	0.016
Bir.	20	1	15	230	0.004	0.011	0.011

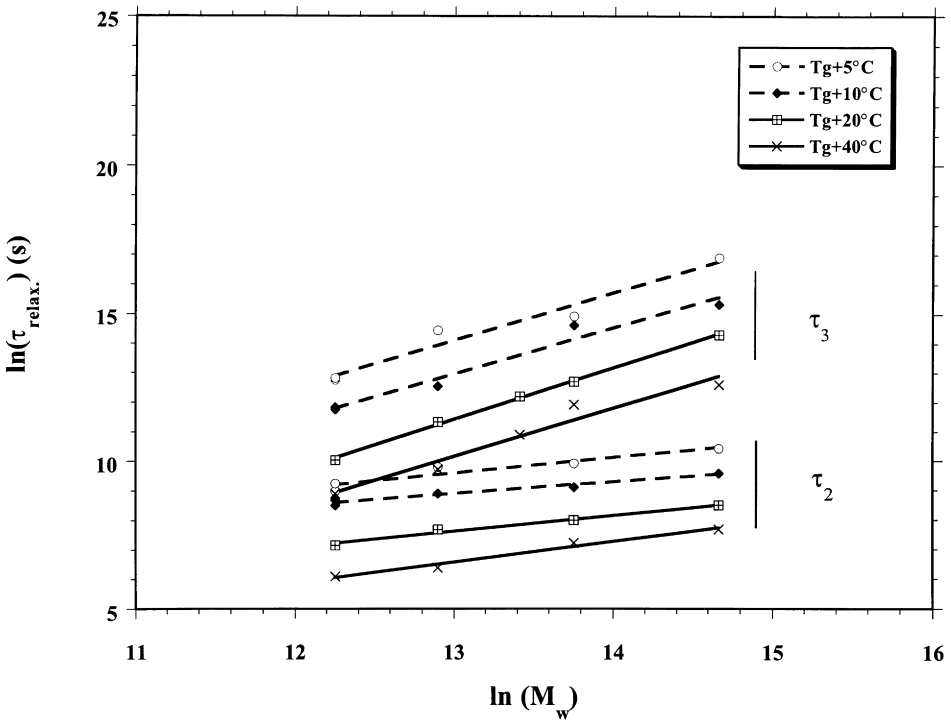

Fig. 11. Evolution of the second and third relaxation times as a function of average molecular weight, at four different temperatures. Please note that the measurements at $T_g + 5$ and $T_g + 10$ were made with the mechanical stretcher whereas those at $T_g + 20$ and $T_g + 40$ were made with the pneumatic stretcher.

where T is the temperature, A, B and T_∞ are empirical constants, and i varies from 1 to 3. T_∞ corresponds to the temperature for which no mobility is observed for the process considered [53,54]. The decay of the third relaxation time with temperature for the different PS samples is similar, and these curves can be superimposed by a vertical translation. From this master curve, Eq. (5) and the $T_g - T_\infty$ value of 51.6 K given in the literature [55], a B

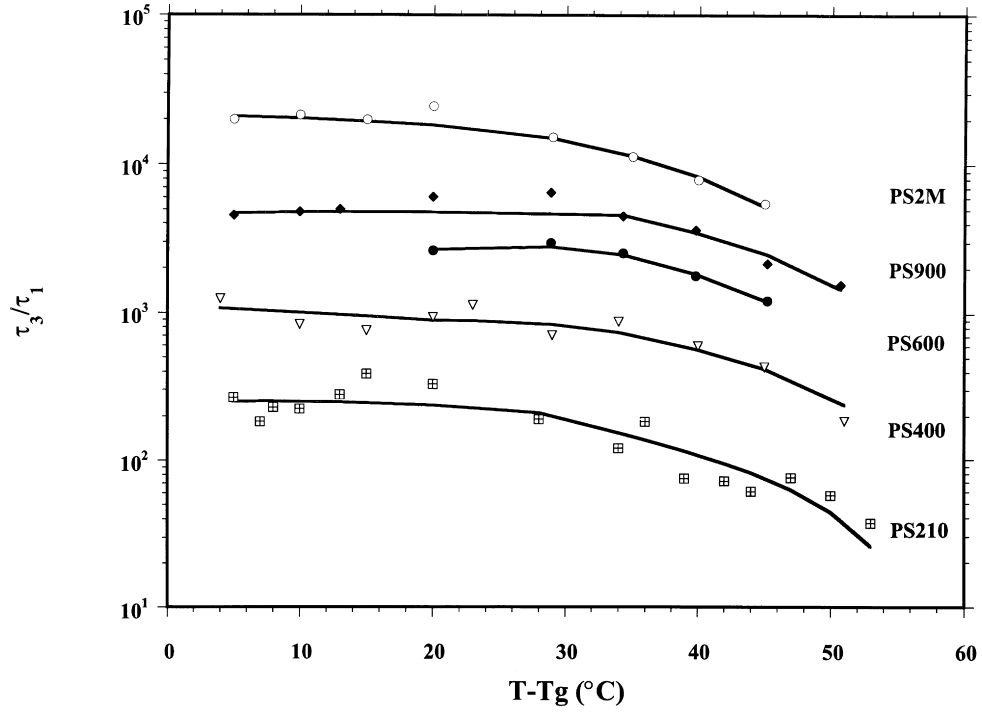

Fig. 12. Variation of the relaxation time ratio, τ_3/τ_1, as a function of temperature, for different PS molecular weights.

value of 540 ± 40 was determined. From the original curves of τ_3, the variation of A can be expressed as a function of the molecular weight by the following equation: $A = 3.7 \ln(M_w) - 48$ with $R^2 = 0.97$. For the first relaxation time (Fig. 10), the B value is equal to 460 ± 20 and A to 1.4.

As an example, for the polydisperse PS sample, relaxation times and pre-exponential parameters are reported in Table 2 (average of at least five independent measurements for each temperature). A number of observations can be made. First, it is seen that there is fair agreement, in all cases but one, between the values found from the birefringence curves and those determined by infrared spectroscopy (the only real difference beyond experimental error is found for τ_3 at $T_g + 8$°C). Second, in all cases, τ_1 is of the order of 1–10 s, τ_2 of 50–100 s and τ_3 of 1000–4000 s. In general, A_1 is slightly larger than A_2 and A_3 at lower temperatures but becomes smaller at $T_g + 20$°C. A_2 and A_3 are always similar.

The variation of the second and third relaxation times as a function of the PS average molecular weight, M_w, is shown in Fig. 11 on a log–log scale, at four different temperatures above T_g. In every case, a linear relationship is observed. From the average of the slopes of the lines of Fig. 11 at $T_g + 5$, $T_g + 10$, $T_g + 20$ and $T_g + 40$°C, it is foundthat $\tau_2 \propto M_w^{0.5\pm0.1}$ and $\tau_3 \propto M_w^{1.6\pm0.1}$. The relaxation time–molecular dependence determined for τ_2 and τ_3 is independent of the stretcher used and polydispersity of the sample.

The relaxation time ratio, τ_3/τ_1, is shown in Fig. 12 as a function of temperature, for each PS sample, on a semi-logarithmic scale. For temperatures close to T_g, a plateau is observed, followed by a gradual decrease between $T_g + 30$ and $T_g + 55$°C. This decrease can be explained by a decrease in the number of entanglement points per chain (chain slippage) or to an increase in the molecular weight between entanglements when considering the Doi–Edwards model. It is consistent with the fact that when the temperature increases, polymer fluidity increases.

The relaxation times reported in this paper are the average of at least five measurements. The experimental error on the determination of τ_1,τ_2 and τ_3 is of about ±0.2, ±3 and ±40 s, respectively, above $T_g + 20$°C; below this temperature, it is larger, particularly for τ_1, due to the stretcher used. With the mechanical stretcher, good repeatability is obtained close to T_g whereas, with the pneumatic device, it is for a temperature close to $T_g + 20$°C that the most repeatable results are obtained. The relative uncertainty on τ_3 decreases with an increase in molecular weight.

The first relaxation time measured here is of the same order of magnitude than that calculated by Tassin et al. [18] from stress–strain curve considerations using the Doi–Edwards model while Tassin and Monnerie [15] reported a value of 5.6 s, at $T_g + 15$°C, from time–temperature superposition, in fair agreement with our experimental value for τ_1 of 2 ± 1 s obtained at the same temperature. It is estimated, using the Doi–Edwards theoretical scaling laws, that the first relaxation time τ_a should lie between 0.8 and 11 s [15,19]. Also, from deformation curves, Abtal and Prud'homme [16] have indirectly calculated, over a broad temperature range and for a monodisperse PS of molecular weight of 300 000, three relaxation times, assuming the validity of the Doi–Edwards model. They found, for example at $T_g + 4$°C, values of 4, 2270 and 120 000 s for τ_a, τ_b, τ_c, respectively. Similarly, Walczak and Wool [6] have determined, from both infrared and chain diffusion studies, retraction and reptation times of PS, at $T_g + 20$°C, and then calculated τ_a; they reported, for a monodisperse PS of molecular weight of 233 000, values of 0.5, 85 and 3280 s for τ_a, τ_b, τ_c, respectively. More recently, Hayes et al. [8] reported, at $T_g + 12$°C, for a monodisperse PS of molecular weight of 188 000 studied by infrared and small-angle neutron scattering, values of 3700 and 100 000 s for τ_b and τ_c.

The analysis of the data of Fig. 10 and Table 2 indicates that τ_3 agrees with the τ_b value reported in Walczak and Wool [6], Hayes et al. [8], and Prud'homme and Abtal [16]. Let us recall that, in the Doi–Edwards model [56], τ_a, τ_b and τ_c correspond to the segmental relaxation between entanglements through fast Brownian motions, to the chain retraction within its deformed tube and to the chain reptation process, respectively. According to the preceding comparisons, it seems reasonable to consider that τ_1 and τ_3 correspond to τ_a and τ_b, respectively, in the Doi–Edwards model. However, in that context, the second relaxation time τ_2, which does not agree with the second relaxation times of Doi–Edwards calculated by Walczak and Wool [6], Hayes et al. [8] and Boué et al. [19], or with those calculated by Prud'homme and Abtal [16] from indirect experimental data, cannot be interpreted by the Doi–Edwards model. It must be assigned to another process such as the partial relaxation of chain ends before the full retraction of the chain centers. From the Tassin and Monnerie studies [15,40], it is known that the chain ends possess a different mobility than the central part of the chain and relax before it. It can be assumed that, before the retraction of the central part occurs, part of the chain ends have already retracted. This simple explanation might be tested through the relaxation study of tri-block deuterated PS whose central position or chain ends are deuterated. The increase of τ_2 observed here with an increase of molecular weight might be attributed to the decrease of the number of chain ends in the PS samples. As the molecular weight increases, the contribution of the chain ends on the relaxation time (τ_2) decreases with the decrease of total free volume added by the chain extremities, through the decrease of the number of chain ends.

In their theoretical model of chain relaxation in polymer melts and concentrated solutions, Doi and Edwards [56,57] postulated that:

$$\tau_a \propto M_w^0 \qquad \text{and} \qquad \tau_b = 2\tau_a(M_w/N_e)^h \tag{6}$$

where M_w is the sample weight-average molecular weight

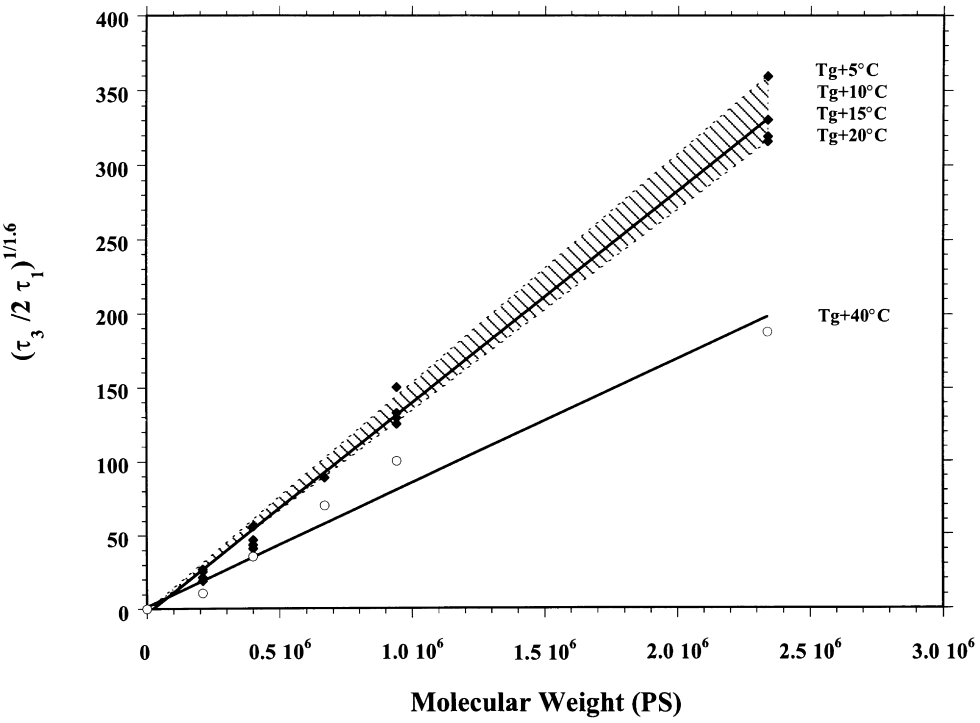

Fig. 13. Determination of the PS molecular weight between entanglements from consideration of the Doi–Edwards model ($\tau_3 = 2\tau_1(M_w/N_e)^{1.6}$) below and at $T_g + 20$°C, and at $T_g + 40$°C.

and N_e, the molecular weight between entanglements. In that study, they obtained $h = 2$ using the Rouse model. However, if the Rouse model is replaced by the Zimm model, where the hydrodynamic interactions are considered, then $h = 3/2$ [56]. If the model proposed by Doi and Edwards is considered to explain the relaxation time variation with molecular weight shown in Fig. 11, it is first noticed that the first relaxation time, τ_1, is independent of molecular weight as predicted, whereas the third relaxation time, τ_3, varies as $M_w^{1.6\pm0.1}$, in agreement with the $M_w^{1.5}$ dependence predicted using the Zimm model. The first and third relaxation times determined here can, therefore, be assigned to the first and second relaxation processes postulated by Doi and Edwards. Furthermore, Tassin et al. [18] reported from stress-strain measurements, at $T_g + 28$°C, a 1.9 ± 0.1 exponent for τ_b, assuming the validity of the Doi–Edwards model, not too far from the 1.6 exponent found here.

In order to further verify this model, from a rearrangement of Eq. (6), the dependence between the relaxation time ratio and the sample molecular weight is expressed as follows:

$$\left(\frac{\tau_b}{2\tau_a}\right)^{1/h} = \frac{M_w}{N_e} \tag{7}$$

This experimental relaxation time ratio, $((\tau_3/2\tau_1)^{1/1.6})$, determined at four different temperatures below $T_g + 20$°C, and at $T_g + 40$°C (Fig. 10), is plotted in Fig. 13 as a function of the PS average molecular weight. The two linear dependencies found indicate the validity of Eq. (7) and of the Doi–Edwards predictions. From the slopes of the lines shown in Fig. 13 and Eq. (7), the molecular weights between entanglements at and below $T_g + 20$, and at $T_g + 40$°C, are determined to be 7000 ± 1000 and $12\,000 \pm 1000$, respectively. These values are smaller than the 13 500 value reported for PS at $T_g + 35$°C [55] and the 18 700 value reported at $T_g + 85$°C [58]. However, the value found here at $T_g + 40$°C and that reported in the literature at $T_g + 35$°C are similar.

As also shown in Fig. 12, the relaxation time ratio τ_3/τ_1 exhibits a similar decrease as a function of temperature, above $T_g + 30$°C, for all the PS samples. In the Doi–Edwards model, as shown in Eq. (7), the τ_b/τ_a ratio is inversely proportional to N_e, suggesting that the decrease of τ_3/τ_1 (or τ_b/τ_a) can be due to an increase of the molecular weight between entanglements (i.e. the loss of entanglements points via chain slippage) with temperature. The chain slippage might be driven by a decrease of the friction coefficient ζ with the temperature but this parameter does not show up directly in Eq. (7) since both τ_a and τ_b are proportional to ζ. Since it is noted that the magnitude of τ_3/τ_1 decay is identical for the low and high molecular weight samples, it cannot be associated with the relaxation processes of the chain ends.

5. Conclusion

The relaxation of five different PS samples, four mono-

disperse and one polydisperse, were studied as a function of temperature, between $T_g + 4$ and $T_g + 60$°C, and draw rate with the birefringence and polarization modulation techniques. These two techniques lead to similar relaxation curves and relaxation times. Relaxation times of 0.7, 39 and 16 500 s were obtained for a monodisperse PS of average molecular weight 2 340 000 at $T_g + 20$°C. τ_1 is molecular weight independent, whereas τ_2 and τ_3 scale as $M_w^{0.5}$ and $M_w^{1.6}$. This behavior for τ_1 and τ_3 is consistent with the Doi–Edwards theory when the hydrodymamic interactions are considered.

Acknowledgements

The authors thank the Natural Sciences and Engineering Research Council of Canada (NSERC) and the Department of Education of the Province of Québec (FCAR) for financial support of this project. They also acknowledge useful discussions concerning the PM-IRLD technique with Thierry Buffeteau (University of Bordeaux; France), concerning the relaxation data with Prof. Gary Slater (University of Ottawa; Canada) and contributions of François Perrault to the development of the birefringence apparatus.

References

[1] Osaki K, Kurata M. Macromolecules 1980;13:671.
[2] Lin YH. Macromolecules 1984;17:2846.
[3] Antonietti M, Coutandin J, Sillescu H. Macromolecules 1986;19:793.
[4] Watanabe H, Kotaka T. Macromolecules 1987;20:530.
[5] Watanabe H, Kotaka T. Macromolecules 1987;20:535.
[6] Walczak WJ, Wool RP. Macromolecules 1991;24:4657.
[7] Hayes C, Mendes E, Bokobza L, Boué F, Monnerie L. Macromol Symp 1995;94:227.
[8] Hayes C, Bokobza L, Boué F, Mendes E, Monnerie L. Macromolecules 1996;29:5036.
[9] Fajolle R, Tassin JF, Sergot P, Pambrun C, Monnerie L. Polymer 1983;24:379.
[10] Lee A, Wool RP. Macromolecules 1986;19:1063.
[11] Tassin JF, Baschwitz A, Moise JY, Monnerie L. Macromolecules 1990;23:1879.
[12] Siesler HS, Hayes C, Bokobza L, Monnerie L. Macromol Rapid Commun 1994;15:467.
[13] Saito H, Takahashi M, Inoue T. J Polym Sci: Polym Phys: Part B 1988;26:1761.
[14] Saito H, Miyashita H, Inoue T. Macromolecules 1992;25:1824.
[15] Tassin JF, Monnerie L. Macromolecules 1988;21:1846.
[16] Abtal E, Prud'homme RE. Polymer 1993;34:4661.
[17] Abtal E, Prud'homme RE. Macromolecules 1994;27:5780.
[18] Tassin JF, Thirion P, Monnerie L. J Polym Sci: Polym Phys Ed 1983;21:2109.
[19] Boué F, Nierlich M, Jannink G, Ball RC. J Phys (Paris) 1982;43:137.
[20] Marrucci G, Hermans JJ. Macromolecules 1980;13:380.
[21] Thirion P, Tassin J. J Polym Sci: Polym Phys Ed 1983;21:2107.
[22] Viovy JL. J Physique 1985;46:847.
[23] Des Cloizeaux J. Macromolecules 1990;23:3992.
[24] De Gennes PG. J Chem Phys 1971;55:572.
[25] Doi M, Edwards SF. J Chem Soc, Faraday Trans 2 1978;74:1789.
[26] Doi M, Edwards SF. J Chem Soc, Faraday Trans 2 1978;74:1802.
[27] Doi M, Edwards SF. J Chem Soc, Faraday Trans 2 1978;74:1818.
[28] Doi M, Edwards SF. J Chem Soc, Faraday Trans 2 1979;75:38.
[29] Kemp JC. J Opt Soc Am 1969;59:950.
[30] Chabay I, Holzwarth G. Appl Optics 1975;14:454.
[31] Nafie LA, Diem M. Appl Spectrosc 1979;33:130.
[32] Hipps KW, Crosby GA. J Appl Phys 1979;83:555.
[33] Wang B. American Laboratory 1996;April:36C.
[34] Buffeteau T, Pézolet M. Appl Spectrosc 1996;50:948.
[35] Buffeteau T, Natansohn A, Rochon P, Pézolet M. Macromolecules 1996;29:8783.
[36] Buffeteau T, Desbat B, Bokobza L. Polymer 1995;36:4339.
[37] Messé L. PhD thesis. Université Laval, Québec, Canada, 1998.
[38] Jasse B, Koenig JL. J Polym Sci: Polym Phys Ed 1979;17:799.
[39] Lefebvre D, Jasse B, Monnerie L. Polymer 1983;24:1240.
[40] Tassin JF, Monnerie L, Fetters L. Macromolecules 1988;21:2404.
[41] Kawabata K, Fukuda T, Tsuji Y, Miyamoto T. Macromolecules 1993;26:3980.
[42] Bazuin CG, Fan XD, Lepilleur C, Prud'homme RE. Macromolecules 1995;28:897.
[43] Samuels R. Structured polymer properties. London: Wiley, 1974.
[44] Ward IM. Development in oriented polymers—2. Amsterdam: Elsevier, 1987.
[45] Kumar S, Stein RS. J Appl Polym Sci 1987;34:1693.
[46] Buffeteau T, Desbat B, Pézolet M, Turlet JM. J Chim Phys (Paris) 1993;90:1467.
[47] Buffeteau T, Desbat B, Besbes S, Nafati M, Bokobza L. Polymer 1994;35:2538.
[48] Lefebvre D, Jasse B, Monnerie L. Polymer 1982;23:706.
[49] Abtal E. PhD thesis. Université Laval, Québec, Canada, 1990.
[50] Stein RS. J Appl Phys 1961;32:1280.
[51] Shaw SJ. Mater Sci Technol 1987;3:589.
[52] Wool RP. Polymer interfaces. New York: Hanser, 1995.
[53] Matsuoka S. Relaxation phenomena in polymers. New York: Hanser, 1992.
[54] Strobl G. The physics of polymers. 2nd ed.. Berlin: Springer, 1997.
[55] Mark JE. Physical properties of polymers handbook. New York: AIP Press, 1996.
[56] Doi M, Edwards SF. The theory of polymer dynamics. Oxford: Clarendon Press, 1986.
[57] Janeschitz-Kriegl H. Polymer melt rheology and flow birefringence. Berlin: Springer, 1983.
[58] Wu S. J Polym Sci: Polym Phys Ed 1989;27:723.